

I. Joining of Dissimilar Metals for Automotive Applications: From Process to Performance

Principal Investigator: Moe Khaleel

Pacific Northwest National Laboratory

P.O. Box 999/K9-95, Richland, WA 99352

(509) 375-2438; fax: (509) 375-6605; e-mail: moe.khaleel@pnl.gov

USCAR Joining Team Contact: Jim Quinn

GM R&D Planning

30500 Mound Rd., MC 480-106-212, Warren, MI 48090-9055

(248) 680-4732; fax: (248) 680-2874; e-mail: james.f.quinn@gm.com

Technology Area Development Manager: Joseph A. Carpenter

(202) 586-1022; fax: (202) 586-1600; e-mail: joseph.carpenter@ee.doe.gov

Field Technical Manager: Philip S. Sklad

(865) 574-5069; fax: (865) 576-4963; e-mail: sklads@ornl.gov

Contractor: Pacific Northwest National Laboratory

Contract No.: DE-AC06-76RL01830

Objective

- Develop and evaluate different technologies for joining dissimilar aluminum alloys and aluminum to steel.
- Characterize the performance of these joints.
- Develop a unified modeling procedure to represent these joints in vehicle structural simulation. The steel materials include mild, high-strength, low-alloy, and dual-phase steels.

Approach

- Further develop and/or enhance self-piercing rivets (SPRs) and resistance spot welding (RSW), with and without adhesives, for joining dissimilar metals.
- Develop a database for the static, dynamic, fatigue, and corrosion behavior of dissimilar material joints, consisting of different material selections and different joining techniques.
- Incorporate and represent the joint performance data into current computer-aided engineering (CAE) codes for evaluation of impact and fatigue performances of joint components.
- Develop design guidelines in the forms of tables and charts for use in joint structural and crash design.

Accomplishments

- Joined high-strength steel (HSLA 350 and DP 600) and 5000-series aluminum alloy specimens, using self-piercing rivets with adhesive (DOW Betamate 4601).
- Accomplished spot welding of dissimilar metals (mild steel and 5000-series aluminum alloy), using a transition material (aluminum-clad steel strip).

- Conducted salt spray corrosion tests (according to ASTM B117) on all current and past populations evaluated. All SPR and RSW joints were exposed for 500 h and examined using both scanning electron microscopy (SEM) and electron dispersive x-ray spectroscopy (EDS).
- Applied the analytical method developed for estimating rivet strength for similar and dissimilar materials to Joint ID 12. The rivet length was increased from 6 mm to 6.5 mm to determine the effect on the joint performance .
- Investigated experimentally the static, fatigue, and dynamic behavior of several combinations of joined dissimilar materials:
 - Joint ID 10A: SPR 5182-O (2 mm) and HSLA 350 (1 mm) with Betamate adhesive
 - Joint ID 11: SPR HSLA (1 mm) and 5182-O (2 mm)
 - Joint ID 11A: SPR HSLA 350 (1 mm) and 5182-O (2 mm) with Betamate adhesive
 - Joint ID 12A: SPR 5182-O (2 mm) and DP 600 (1.6 mm) with Betamate adhesive plus 6.5-mm rivet
 - Joint ID 12L: SPR 5182-O (2 mm) and DP 600 (1.6 mm) with 6.5-mm rivet
 - Joint ID 13: SPR DP 600 (1.6 mm) and 5182-O (2 mm)
 - Joint ID 16: RSW 1008 (1.4 mm) and 5182-O (2 mm) with aluminum clad steel interlayer (1.5 mm)
- Conducted mechanical and microstructural evaluation of dissimilar metal joints subjected to static, dynamic, and fatigue loads. Also investigated the effects of structural adhesives, temperature, piercing direction, dissimilar materials combinations, and loading rates.
- Developed component-level joint fatigue analyses, using experimentally obtained master stress-intensity factor (SIF) life curves.
- Investigated the influence of weld ductility on component crash behaviors.
- Incorporated the joint overload failure criterion.

Future Direction

- Complete joint durability testing of DP600 and 5000-series aluminum alloy specimens in which a group is exposed to 500 h of salt spray/fog and then tested (static and fatigue).
- Transfer joint performance database to members of the joining team.
- Incorporate the proposed failure criterion with software developers.

Introduction

This project is a collaborative effort between DOE, Pacific Northwest National Laboratory, and the Metals Joining Team of the U.S. Council for Automotive Research (USCAR). The work started in April 2001.

The automotive industry envisions that an optimized vehicle, in terms of performance and cost, can be achieved only by using different materials at different vehicle locations to utilize the materials' functionalities to the fullest extent.

Currently, aluminum and steel are the most important construction materials for the mass production of automotive structures. High-volume, nonsteel joining is a significant new problem to the industry. For joining dissimilar aluminum alloys, the leading candidate joining methods are spot welding and SPRs with or without adhesives. The major concerns with aluminum spot welding are its high-energy consumption, low electrode life (see report 7F), and structural performance concerns related to

weld porosity. For joining aluminum to steel, the industry is currently comfortable with SPRs (with and without adhesives). However, there are a number of barriers to the widespread exploitation and high-volume production of the riveting technology. One of these barriers is the limited performance data relative to automotive applications.

In contrast, to shorten the vehicle development cycle, more and more CAE analyses are performed before the actual prototype is built. The question that the CAE engineers ask most often is how to represent the structural joints in crash simulation and fatigue simulation. Currently, there is no unified approach to representing the structural joints that works for different material combinations under multiaxial loading. This is particularly true for dissimilar material joints, where even the basic performance information on the joint coupon level does not exist.

Joint Populations

We experimentally investigated the static, fatigue, and dynamic behavior of several dissimilar material joint populations:

- Joint ID 10A: SPR 5182-O (2 mm) and HSLA 350 (1 mm) with Betamate adhesive
- Joint ID 11: SPR HSLA 350 (1 mm) and 5182-O (2 mm)
- Joint ID 11A: SPR HSLA 350 (1 mm) and 5182-O (2 mm) with Betamate adhesive
- Joint ID 12A: SPR 5182-O (2 mm) and DP 600 (1.6 mm) with Betamate adhesive and 6.5-mm rivet
- Joint ID 12L: SPR 5182-O (2 mm) and DP 600 (1.6 mm) with 6.5-mm rivet
- Joint ID 13: SPR DP 600 (1.6 mm) and 5182-O (2 mm)
- Joint ID 16: RSW 1008 (1.4 mm) and 5182-O (2 mm) with aluminum-clad steel interlayer (1.5 mm)

Static Joint Strength Evaluation

Static tests were performed for three loading configurations for each sample population to derive the overload failure envelope for that population. These three loading configurations are lap shear, cross tension, and coach peel. The results of the static tests were then postprocessed to obtain the peak load, failure displacement, and energy absorption upon failure to validate the proposed energy-based failure criterion. Results from static testing of SPRs of aluminum 5182-O and high-strength steels (HSLA 350 and DP 600) with and without adhesives are compared in Figures 1–4.

The effects of adhesives in SPR joints will be documented in a topical report. The report will include the failure modes of these tests along with an analysis of the static strengths using Weibull probability plots.

Experiments were performed to investigate the effect of rivet length on the static performance of joints. The rivet length of Joint ID 12 (5182-O/DP 600) was increased from 6 mm to 6.5 mm. The same joining parameters were applied (i.e., rivet type, die, pressures). The longer rivet clinches more material and contributes to the performance of the joint. The static results are illustrated in Figure 5.

The effect of piercing direction on the static performance of joints was also evaluated. Joint ID 10 (5182-O/HSLA 350) and Joint ID 11 (HSLA 350/5182-O) are compared in Figures 6 and 7. The same rivet and die design was used to join the two dissimilar materials in each population. It was observed that different piercing directions yield different strength characteristics for the joints.

An annealed aluminum-clad steel interlayer material was used to resistance spot weld 5182-O aluminum with 1008 steel (Joint ID 16). Fatigue, static, and dynamic tests were performed on the RSW joint with the interlayer material. The test data were compared to Joint ID 9 (SPR 1008/5182-O).

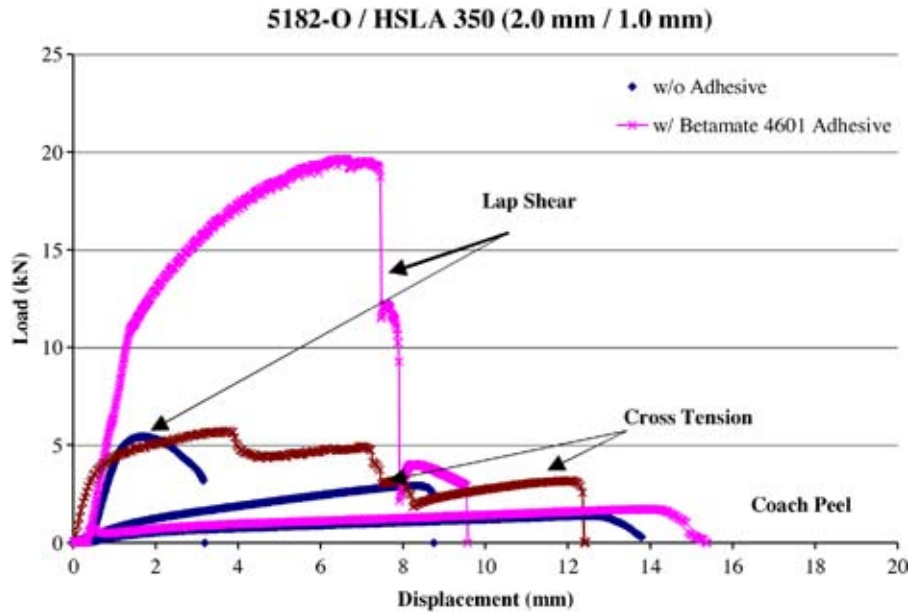


Figure 1. Uniaxial test results for Joint ID 10 and 10A. Results shown are representative of the average peak load observed for the specimen designs tested in each joint population.

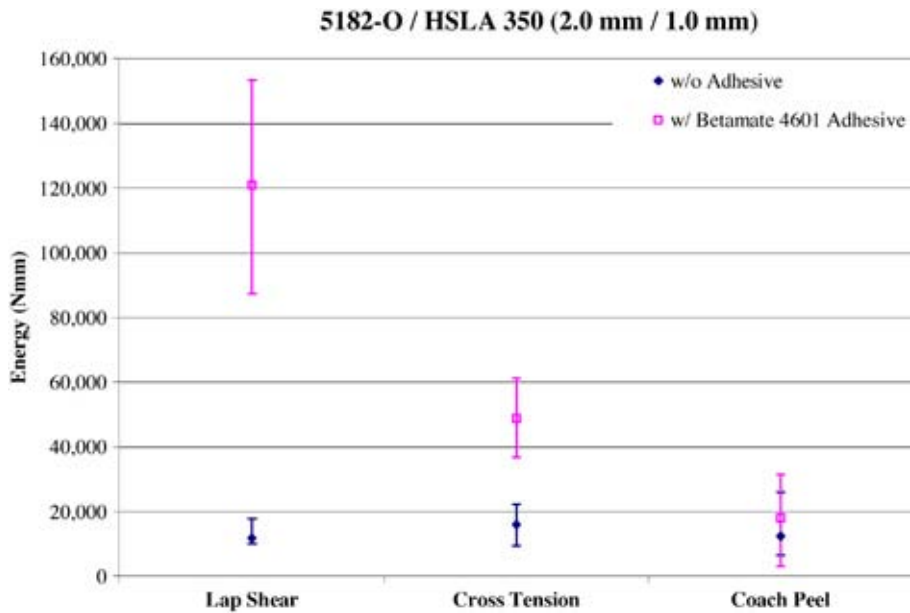


Figure 2. An illustration of the static test energy absorption results for Joint ID 10 and 10A.

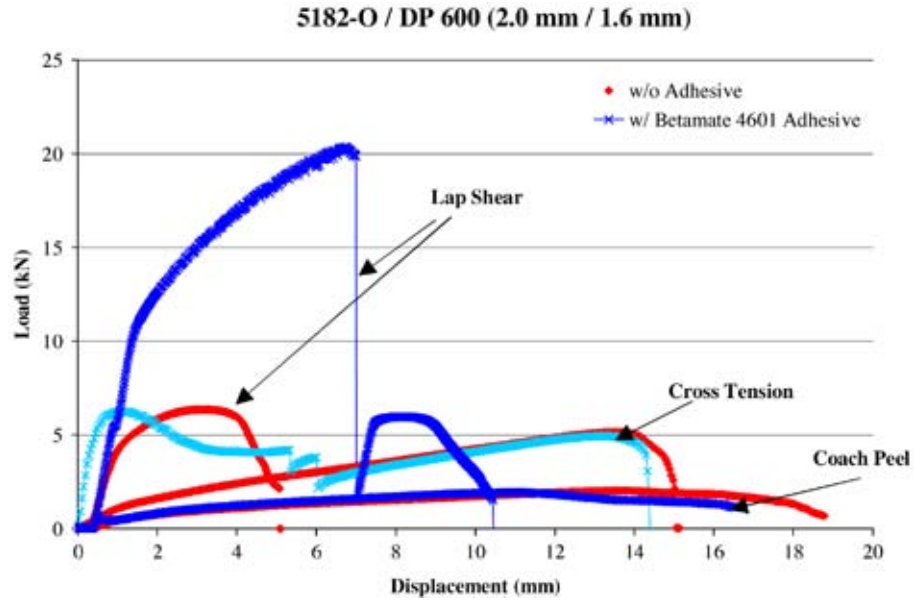


Figure 3. Uniaxial test results for Joint ID 12L and 12A. Results shown are representative of the average peak load observed for the specimen designs tested in each joint population.

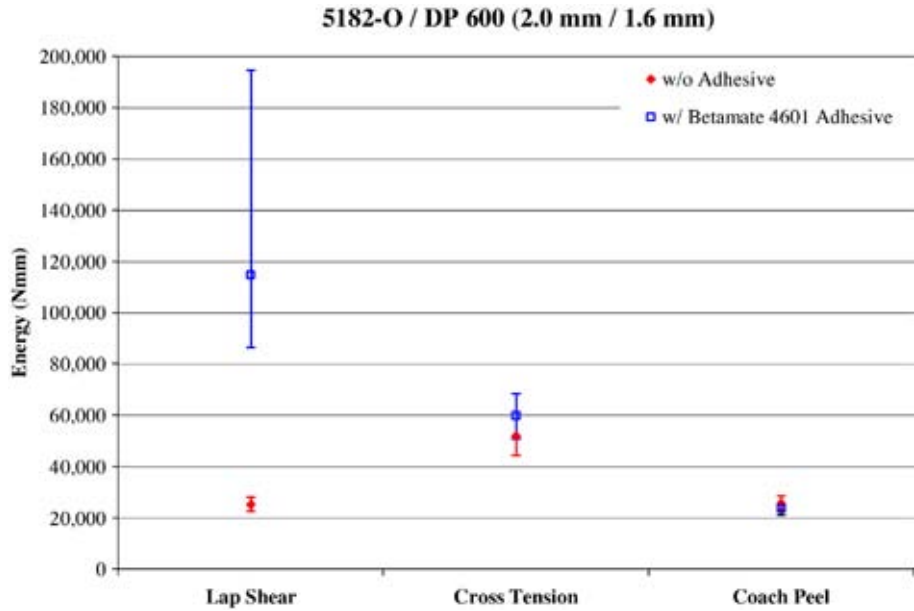


Figure 4. An illustration of the static test energy absorption results for Joint ID 12L and 12A.

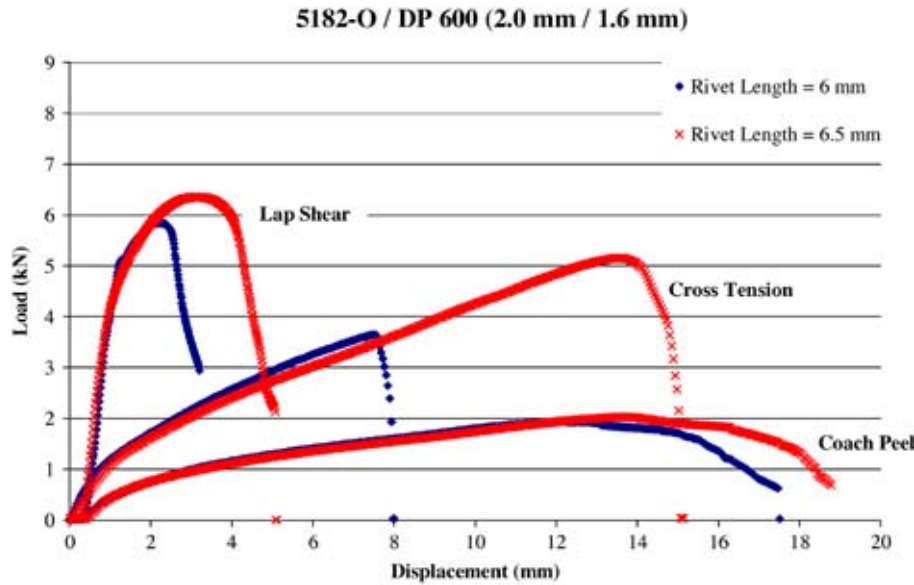


Figure 5. Uniaxial test results for Joint ID 12 and 12L. Results shown are representative of the average peak load observed for the specimen designs tested in each joint population.

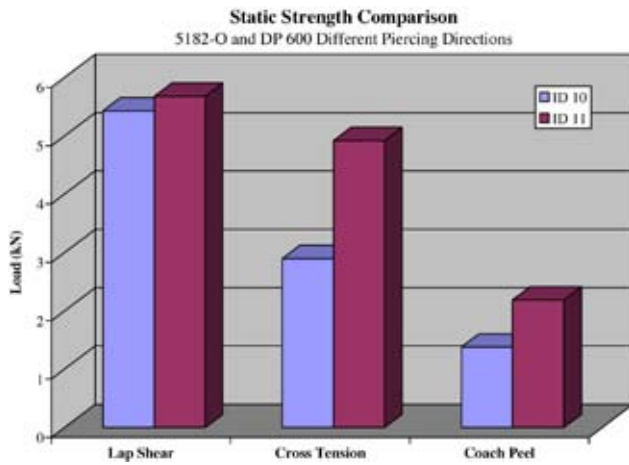


Figure 6. An illustration of the static peak load results for Joint ID 10 and 11. Results shown are representative of the average peak load observed for the specimen designs tested in each joint population.

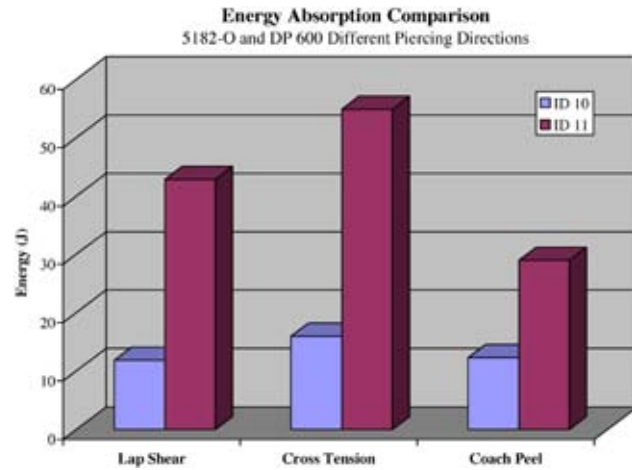


Figure 7. An illustration of the static test energy absorption results for Joint ID 10 and 11. Results shown are representative of the average energy absorption for the specimen designs tested in each joint population.

Figure 8 illustrates the static strength test results for both joint populations.

The development of the interlayer material and utilization of this material to RSW aluminum with steel was documented in a topical report, *Resistance Spot Welds of Aluminum Alloy to Steel with Transition Material—From Process to Performance*. This report characterized the RSW joint from process to performance and compared its performance with Joint ID 9. The report included the failure modes of these tests along with an analysis of the static strengths. These failure modes and static strength data can help the designer of a lightweight vehicle choose the correct material combinations for desired static vehicle performance.

Dynamic Joint Strength Evaluation

Dynamic impact tests of 10 mph and 20 mph were performed on all sample populations under three loading configurations. Example results of cross tension for ID 10A are shown in Figure 9. To determine the dynamic strength accurately,

two sets of unique lightweight fixtures were designed for the coupon configurations. These fixtures are rigid, and they connect themselves directly to the piezoelectric load cell, thereby eliminating the possibility of a fictitious load signal resulting from inertia effects. The rigidity, or compliance, of the testing frame was also adjusted prior to the dynamic tests to ensure that the test frame is rigid enough that its natural frequency is much higher than the response frequency of the tested sample. Ringing effect was thus minimized to the greatest extent possible. The dynamic test results were then postprocessed to obtain the peak load, failure displacement, and energy absorption upon failure to populate the failure envelope and to validate the proposed energy-based failure criterion.

Figure 10 illustrates the loading rate effect of Joint ID 11 under cross tension loading condition. It shows that under dynamic loading conditions, displacement to failure decreases with increasing loading rate; however, the peak failure load remains relatively unchanged from the static

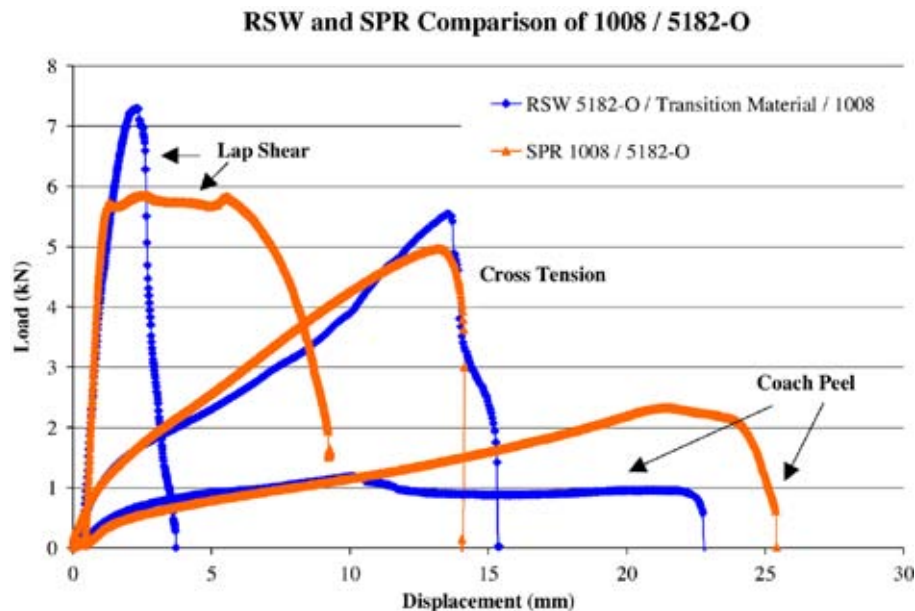


Figure 8. Uniaxial test results for SPR Joint ID 9 and RSW Joint ID 16. Results shown are representative of the average peak load observed for the specimen designs tested in each joint population.

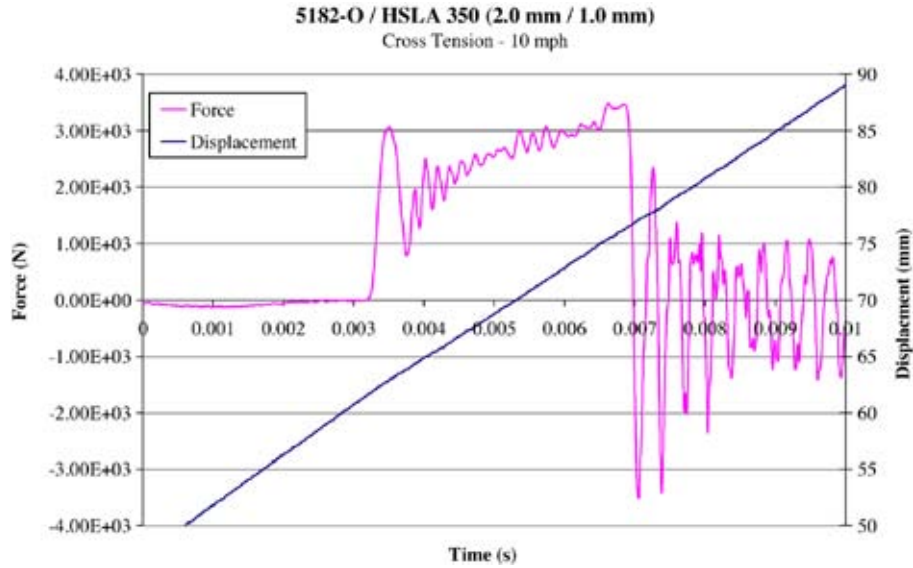


Figure 9. Dynamic test results for Joint ID 10A.

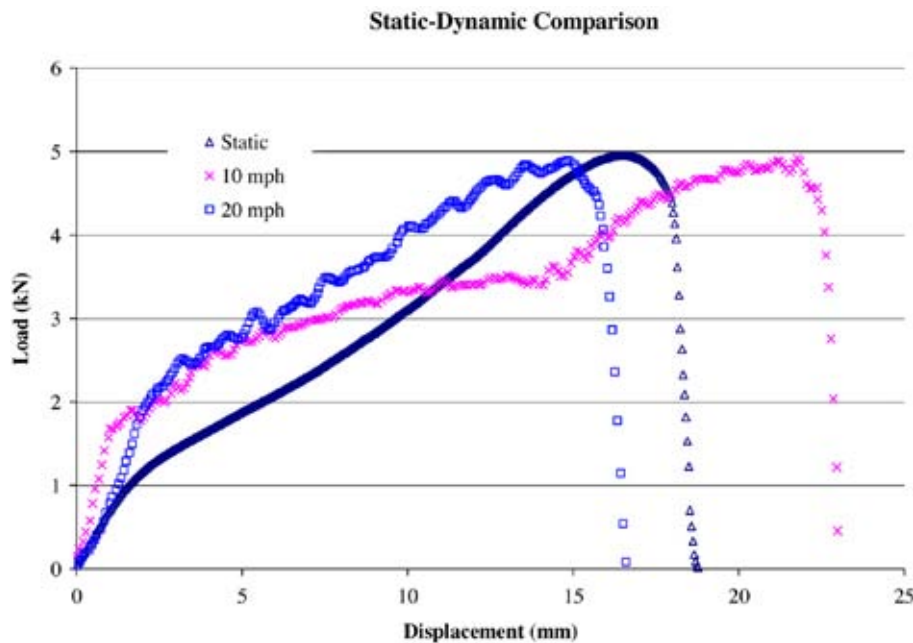


Figure 10. Illustration of the loading rate effect on Joint ID 11 under cross tension loading.

level. Similar conclusions can be drawn for other joint populations with aluminum as the base material. These dynamic results indicate that the total energy absorption for the joint samples decreases with increasing testing velocity. This is because the joints fail in a shorter grip distance due to geometric constraints and inertia effects of the

surrounding sheet metal at high loading rates.

The failure modes of these dynamic tests will also be documented in the topical reports. The failure mode and dynamic strength data can help the designer to select materials for desired dynamic performance.

Joint Fatigue Strength Evaluation

Cyclic fatigue tests were performed on all sample populations under a tension-tension ratio of $R = 0.1$. Fatigue tests were conducted on all specimen designs (lap shear, cross tension, and coach peel). It was found that the coach peel coupons exhibit the lowest fatigue life for the three coupon configurations because of the high stress

concentrations for this loading condition. Among the three loading conditions, lap shear had the highest fatigue life. Example results of fatigue data comparing SPR joints with and without adhesives are shown in Figure 11, and fatigue data comparing RSW Joint ID 16 and SPR Joint ID 9 are shown in Figure 12.

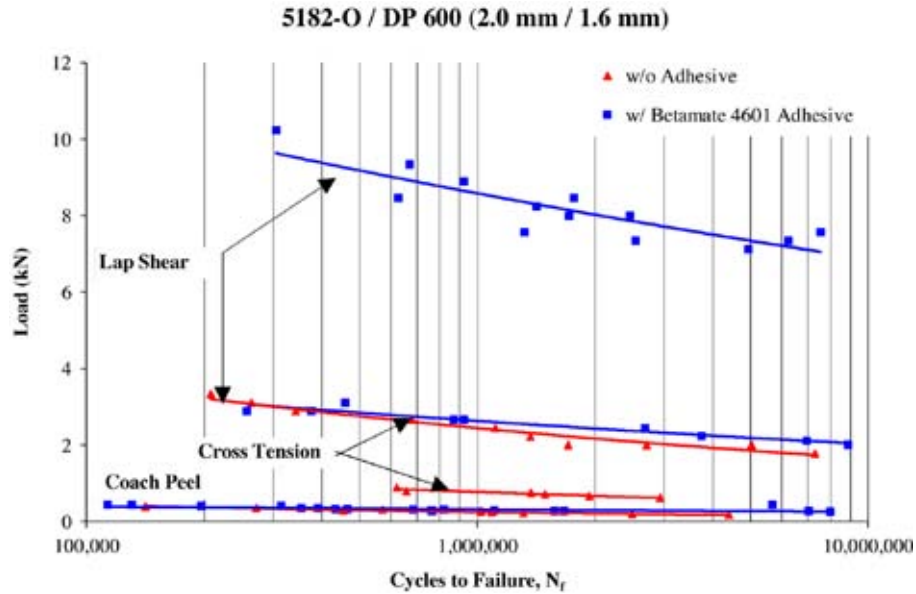


Figure 11. Fatigue test results comparing Joint ID 12L and 12A.

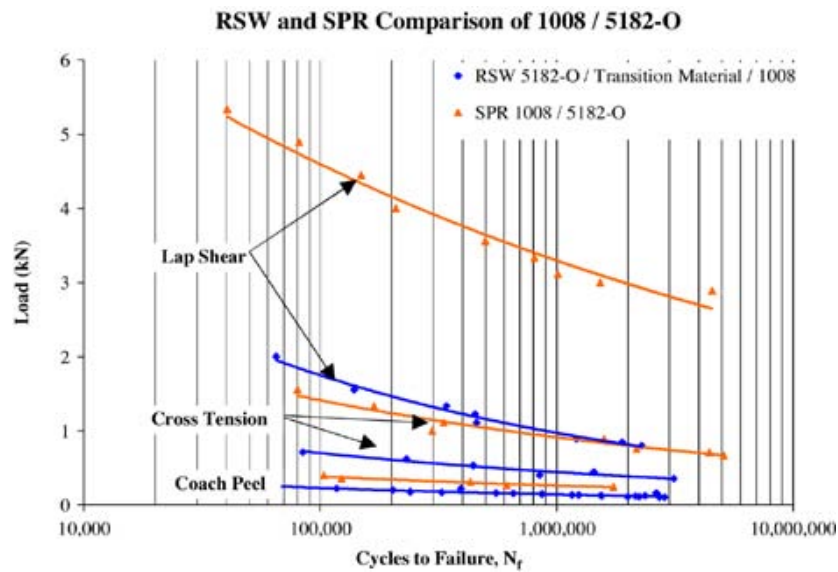


Figure 12. Fatigue test results comparing RSW Joint ID 16 and SPR Joint ID 9.

Joint Corrosion Evaluation

Salt spray corrosion tests were conducted on all current and previous SPR and RSW populations evaluated (with the exception of Joint ID 13 and 16). Specimens were exposed to salt spray/fog for 500 h according to ASTM B117. SEM and EDS were performed to determine whether corrosion was observed in the joints after being exposed to salt spray.

A nontested SPR joint was analyzed to set a baseline for the EDS analysis. It identified the parent substrates, the steel rivet, and the Zn/Sn-Al coating on the rivet. No other significant elements were observed. The same rivet material and rivet coating was used in each varying SPR joint population.

No pitting or crevice corrosion was observed in any of the populations analyzed. However, chloride and increased levels of oxygen were present in all SPR populations tested without adhesive in the joint. No chloride was present in the RSW joints or the SPR joints with adhesive.

Figure 13 is an EDS graph that is representative of the typical elements observed at the rivet interface in all SPR populations analyzed without adhesive. In this particular joint, an EDS analysis was performed at the tail of the rivet where two dissimilar

materials met (5182-O and HSLA 350). The presence of chloride and oxygen was observed at the rivet interface in addition to zinc, tin, and aluminum. Chloride and high levels of oxygen were no longer observed at the tail end of the rivet where it is clinched into the bottom material.

Joint CAE

Development of Fatigue Failure Criterion

Fatigue life-vs-load curves tend to have a very large scatter for different material grades, weld sizes, and material thickness combinations. Even for the same joint population, fatigue life-vs-load curves for different coupon configurations are also different. Therefore, it is difficult to cross compare the fatigue performance of different joint geometries and joint populations, and it is even more difficult to apply the fatigue strength measurement from a coupon-level test to a component-level fatigue life prediction. In this project, SIF was chosen to be used as the single parameter to consolidate the fatigue performance curves of different joint populations and different coupon geometries into the fatigue master SIF-life curves. The SIF was chosen because of

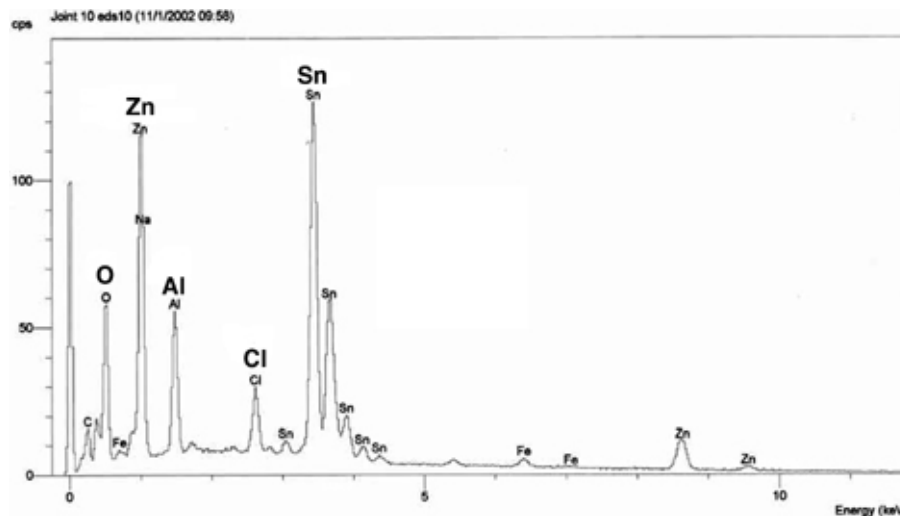


Figure 13. An EDS graph of the rivet interface for Joint ID 10. The EDS graph is typical of the elements observed at the rivet interface in all SPR populations analyzed without adhesive.

its accuracy and computational simplicity in vehicle simulation.

During this reporting period, master SIF-life curves for joints made of different materials and different thickness combinations were also generated using coupon-level fatigue test results under the three different loading conditions. Figure 14 is an example of the master curve for Joint ID 9.

In a component-level fatigue life simulation, the resultant force and moment components for the joint beam element are obtained. The SIF for each joint is calculated based on beam element output, and the corresponding cycle is predicted based on the master SIF-life curve generated.

Development of Overload Failure Criterion

During this reporting period, a force-based failure criterion, Equation (1), was implemented into the dynamic explicit software LS-DYNA. The failure criterion was derived from the static and dynamic test results of different joint coupon configurations.

$$\left(\frac{N_{rr}}{N_{rrF}}\right)^2 + \left(\frac{N_{st}}{N_{stF}}\right)^2 + \left(\frac{M_{st}}{M_{stF}}\right)^2 = 1 \tag{1}$$

Frontal and side impact simulations were then performed to evaluate the impact performance of spot-welded aluminum and steel hat sections. Failure functions were also monitored for each weld during the deformation processes. It was found that the force-based failure criterion was capable of predicting joint failure due to overloading. However, the force-based failure criterion was not capable of distinguishing between brittle and ductile joint failure. For aluminum and steel rails under the same impact condition with the same joint strength, aluminum rails exhibit better energy management characteristics with more progressive folding and less joint failure, see Figures 15 and 16.

Further study is needed in this area to incorporate the strain rate sensitivity of the weld strength into the dynamic simulation package so that the joint element can be eliminated automatically when the joint forces are outside the corresponding failure

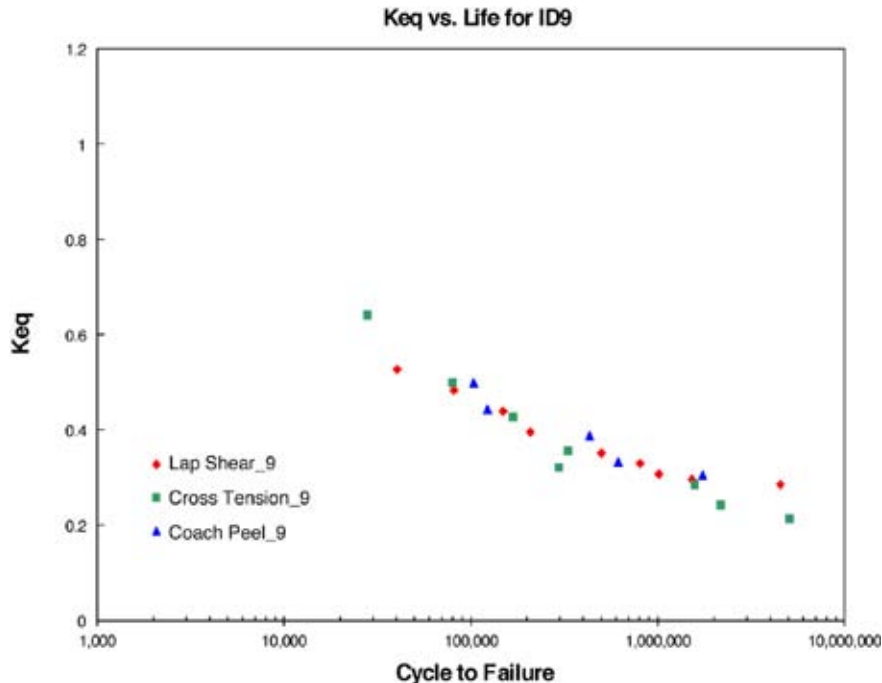


Figure 14. Master SIF curve for Joint ID 9 (SPR 1008/5182-O).

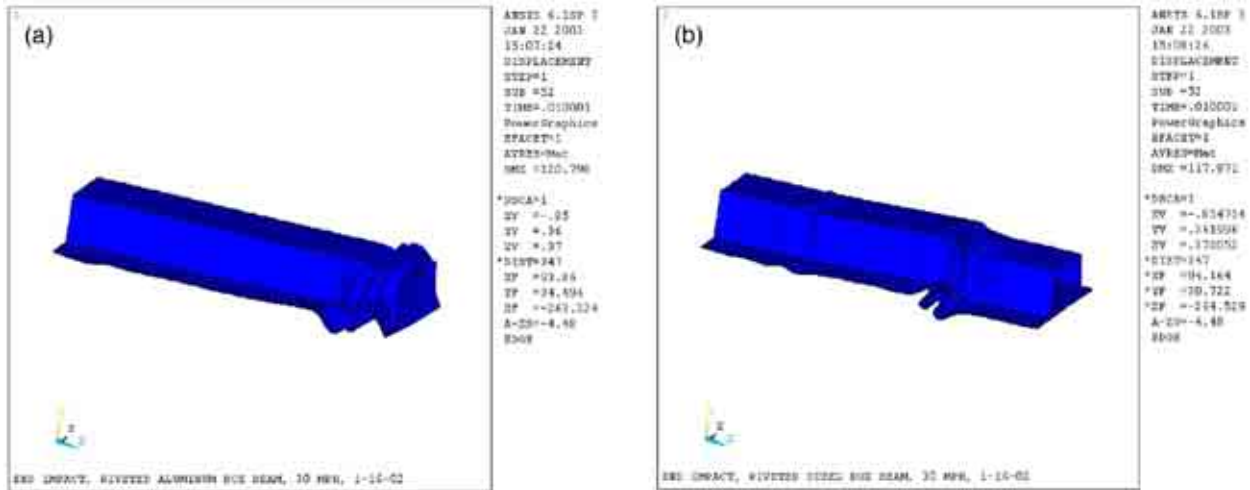


Figure 15. Predicted frontal impact behavior for aluminum and steel hat sections. (a) Aluminum hat section; no weld failure predicted. (b) Steel hat section; two weld failure predicted.

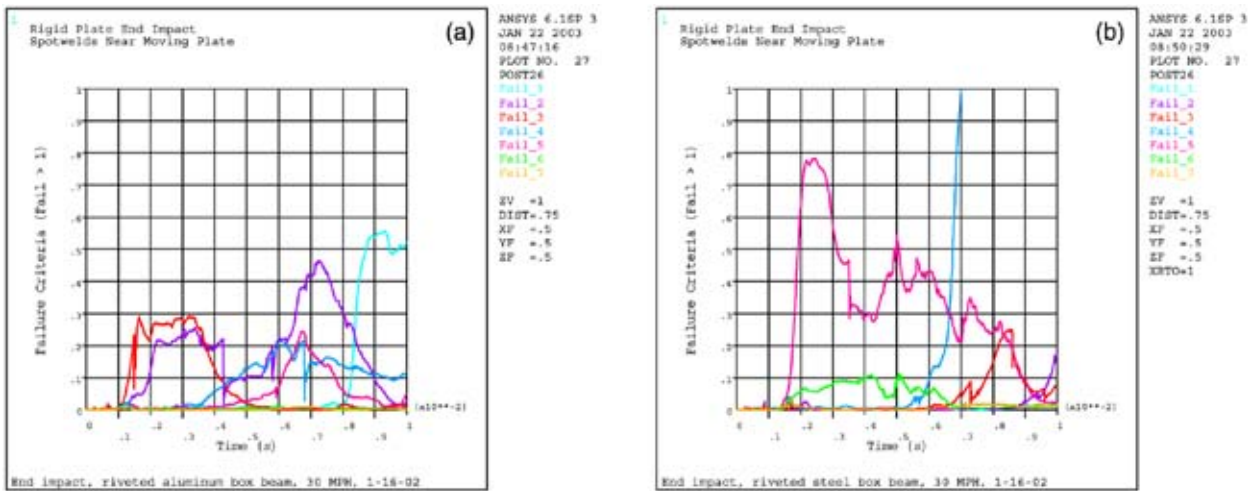


Figure 16. Monitored weld failure functions during impact. (a) Aluminum rail. (b) Steel rail.

envelope. In addition, more work needs to be done to incorporate the energy-based failure criterion in the simulation package.

Meetings

Project review meetings were held on January 31 and September 19, 2003, at the U.S. Council for Automotive Research. Members of the joining team participated.

Reports

The following topical reports were completed and distributed to the Metals Joining Team:

1. *Performance Comparisons through Weibull Analyses of Self-Piercing Rivets and Resistance Spot Welds Joining Dissimilar Metals*
2. *Resistance Spot Welds of Aluminum Alloy to Steel with Transition Material—From Process to Performance*

3. *Characterization of Fatigue Behaviors of Dissimilar Metals Joints Part I—Experimental Studies*
4. *Effect of Failure Modes on Strength of Aluminum Resistance Spot Welds*
5. *Analytical Strength Estimator for Self-Piercing Rivets*
6. *Lap Shear Coupon Design Sensitivity Study for Self-Piercing Rivets and Resistance Spot Welds*